# Colloidal Nanocrystals of Wurtzite-Type Cu2ZnSnS4: Facile Noninjection Synthesis and Formation Mechanism

**ARTICLE** *in* CHEMISTRY - A EUROPEAN JOURNAL · MARCH 2012

Impact Factor: 5.73 · DOI: 10.1002/chem.201103635 · Source: PubMed



**8 AUTHORS**, INCLUDING:

Michelle D Regulacio
Agency for Science, Technology and Resear…
**23** PUBLICATIONS **749** CITATIONS
SEE PROFILE

Enyi Ye
Agency for Science, Technology and Resear…
**45** PUBLICATIONS **517** CITATIONS
SEE PROFILE

Qing-Hua Xu
National University of Singapore
**129** PUBLICATIONS **3,228** CITATIONS
SEE PROFILE

Ming-Yong Han
Agency for Science, Technology and Resear…
**133** PUBLICATIONS **6,536** CITATIONS
SEE PROFILE

DOI: 10.1002/chem.201103635

# Colloidal Nanocrystals of Wurtzite-Type $Cu_2ZnSnS_4$: Facile Noninjection Synthesis and Formation Mechanism

**Michelle D. Regulacio,[a] Chen Ye,[b] Suo Hon Lim,[a] Michel Bosman,[a] Enyi Ye,[a] Shiyou Chen,[c] Qing-Hua Xu,[b] and Ming-Yong Han*[a, d]**

$Cu_2ZnSnS_4$ (CZTS), a quarternary chalcogenide p-type semiconductor, is currently receiving considerable attention as absorber materials for low-cost photovoltaics due to its high absorption coefficient, optimal band gap, and naturally abundant and nontoxic elemental components.[1] The growing technological interest in this material has motivated the study of the nature of its crystal structures.[2] The ground-state crystal structure of CZTS is the kesterite form (space group $I\bar{4}$), which is a tetragonal superstructure derived from the binary II–VI cubic zinc-blende (ZB) lattice. Several other ZB-related structural modifications of CZTS have been considered, and these include the stannite structure (space group $I\bar{4}2m$). This structure type differs from the kesterite form only in the ordering of $Cu^+$ and $Zn^{2+}$ ions. In a recent theoretical study, Chen et al. have shown that there are two low-energy structural configurations of CZTS that are not based on the ZB unit cell.[2f] Instead, these two predicted structures are derivatives of the binary II–VI hexagonal wurtzite (WZ) structure and are conveniently referred to as WZ-kesterite and WZ-stannite, owing to their structural relationship with the ZB-derived kesterite and stannite polytypes, respectively. The WZ-kesterite form is a monoclinic (pseudo-orthorhombic) superstructure of the WZ unit cell and has the space group *Pc*. The WZ-stannite phase, on the other hand, is described by an orthorhombic supercell with space group $Pmn2_1$. In bulk form, WZ-type superstructures have long been reported for a number of quarternary chalcogenides such as $Cu_2MGeS_4$ (in which M = Mn, Zn, Cd).[3] Bulk CZTS with a WZ-derived phase, however, has yet to be synthesized.

In nanocrystalline form, CZTS materials have been colloidally prepared by means of the hot-injection synthetic strategy involving the reaction of the Cu, Zn, and Sn precursors with elemental sulfur in oleylamine at high-temperature conditions.[4] The nanocrystals produced by this method are quite polydisperse in shape and size, and adopt the thermodynamically more stable ZB-derived tetragonal phase. Very recently, Lu et al. have employed the hot-injection technique and used dodecanethiol as the sulfur source in preparing CZTS nanoprisms and nanoplates that are 20–50 nm in size.[5] X-ray diffraction (XRD) measurements revealed that these nanocrystals possess a WZ-related crystal structure. Their proposed structure is based on the hexagonal WZ-ZnS unit cell described by the space group $P6_3mc$, in which the metal cations are randomly distributed in the cation sites (i.e., cation-disordered). However, the possibility that their WZ-type CZTS exhibits the theoretically predicted lower-energy cation-ordered WZ-kesterite and WZ-stannite structures has not been considered.

Herein, we provide a facile noninjection synthetic route to preparing monodisperse anisotropic CZTS nanocrystals that adopt a WZ-type crystal structure. The noninjection or "heating up" approach to colloidal nanocrystals is better in terms of synthetic reproducibility, more convenient for manipulation, and more suitable for large-scale production as compared to the hot-injection method.[6] The XRD pattern of our sample matches well with the simulated pattern of the cation-disordered WZ-type structure proposed by Lu et al. as well as with the simulated patterns of the theoretically predicted cation-ordered WZ-kesterite and WZ-stannite structures. Our study of the formation mechanism reveals that the growth process involves the initial nucleation of a binary copper sulfide phase, which serves as the starting point for the formation of CZTS. As a result, the crystal structure of the generated CZTS is related to the crystal structure of the copper sulfide seed. In addition, we demonstrate a simple route to phase-controlled synthesis of CZTS by varying the organic surfactants used in the synthesis.

The nanocrystals were prepared by thermal decomposition of metal dithiocarbamate complexes (i.e., $[Cu(dedtc)_2]$,

[a] Dr. M. D. Regulacio, Dr. S. H. Lim, Dr. M. Bosman, Dr. E. Ye, Prof. M.-Y. Han
Institute of Materials Research and Engineering
Agency for Science, Technology and Research (A*STAR)
3 Research Link, 117602 (Singapore)
Fax: (+65) 68720785
E-mail: my-han@imre.a-star.edu.sg

[b] C. Ye, Prof. Q.-H. Xu
Department of Chemistry
National University of Singapore
3 Science Drive 3, 117543 (Singapore)

[c] Dr. S. Chen
Laboratory of Polar Materials and Devices
East China Normal University
Shanghai, 200241 (P. R. China)

[d] Prof. M.-Y. Han
Department of Bioengineering
National University of Singapore
9 Engineering Drive 1, 117576 (Singapore)

Supporting information for this article is available on the WWW under http://dx.doi.org/10.1002/chem.201103635.

  

[Zn(dedtc)$_2$] and [Sn(dedtc)$_4$], in which dedtc = $(S_2CNEt_2)^-$ or diethyldithiocarbamate) in a surfactant mixture of hexadecanethiol and trioctylamine at 250 °C (see Experimental Section for details). The representative transmission electron microscopy (TEM) image of the as-prepared nanocrystals shown in Figure 1a reveals that the product consists of

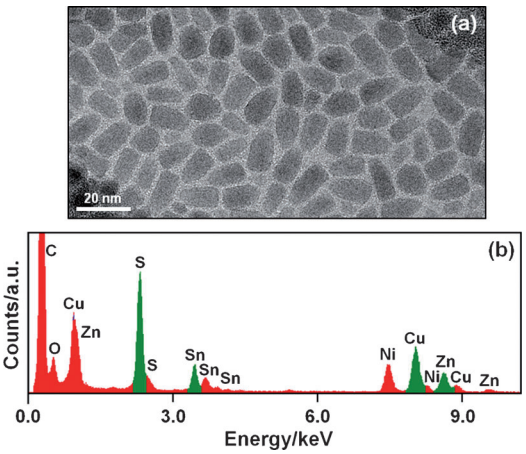


Figure 1. a) TEM image and b) EDX spectrum of the as-synthesized CZTS nanocrystals. Note: In b), the peaks highlighted in green were used to calculate for the elemental composition. The C, O, and Ni signals are attributed to the carbon-coated Ni TEM grid.

elongated nanocrystals with one end (base) being much wider than the other (tip). The nanocrystals are nearly monodisperse, with an average size of (15.1 ± 1.0) nm (length) × (7.6 ± 0.6) nm (base width), as measured from a population of 75 crystallites. The high-resolution TEM images displayed in Figure S1 (in the Supporting Information) reveal continuous lattice fringes, which is indicative of the single-crystalline nature of the nanocrystals. Energy-filtered TEM (EFTEM) images were taken to obtain the elemental distribution maps and these are shown in Figure S2 (in the Supporting Information). It can be seen from the images that Cu, Zn, Sn, and S are homogeneously distributed throughout the nanocrystals. This indicates that binary ($Cu_xS$, ZnS, $SnS_x$) and ternary ($Cu_2SnS_3$) sulfides are not present in the final product.

Energy dispersive X-ray (EDX) spectroscopy and inductively coupled plasma atomic emission spectroscopy (ICP-AES) measurements were performed to determine the elemental composition of the nanocrystals. A typical EDX spectrum is displayed in Figure 1b, in which Cu, Zn, Sn, and S signals are observed. Peak analysis gives a Cu/Zn/Sn/S ratio of 2.10:1.00:0.93:3.86. Elemental analysis by ICP-AES yields a Cu/Zn/Sn metal ratio of 2.00:0.91:1.00. These results are very near the expected Cu/Zn/Sn/S ratio of 2:1:1:4. X-ray photoelectron spectroscopy (XPS) was used to determine the oxidation states of the four constituent elements. The XPS spectra of all four elements are shown in Figure 2. The doublet peaking at 932.7 and 952.6 eV, with a peak splitting of 19.9 eV, is indicative of monovalent Cu. The two

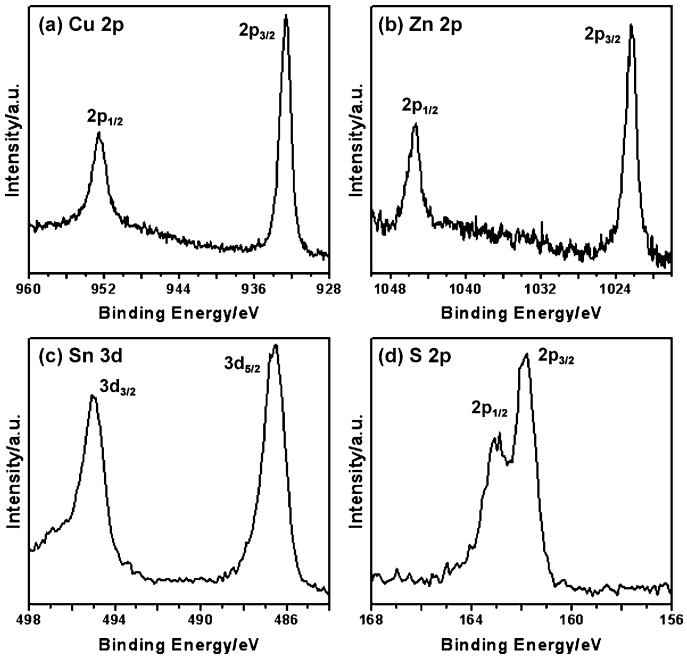


Figure 2. High-resolution XPS analysis of CZTS nanocrystals showing the a) Cu 2p, b) Zn 2p, c) Sn 3d and d) S 2p spectra.

peaks centered at 1022.4 and 1045.3 eV show a peak separation of 22.9 eV, which is consistent with the standard splitting exhibited by divalent Zn. The peaks observed at 486.5 and 495.1 eV, with a peak separation of 8.6 eV, are attributable to tetravalent Sn. The peaks at 161.8 and 162.9 eV are in good accordance with those reported for S in sulfide phases.

The powder X-ray diffraction (XRD) pattern of the as-obtained CZTS nanocrystals is shown in Figure 3a. The diffraction pattern did not match with those reported in the literature for CZTS having the ZB-derived tetragonal structure.[4,7] The similarity of the pattern to that of WZ-ZnS strongly hinted that our nanocrystals might have a WZ-related crystal structure. Lu et al. have observed similar dif-

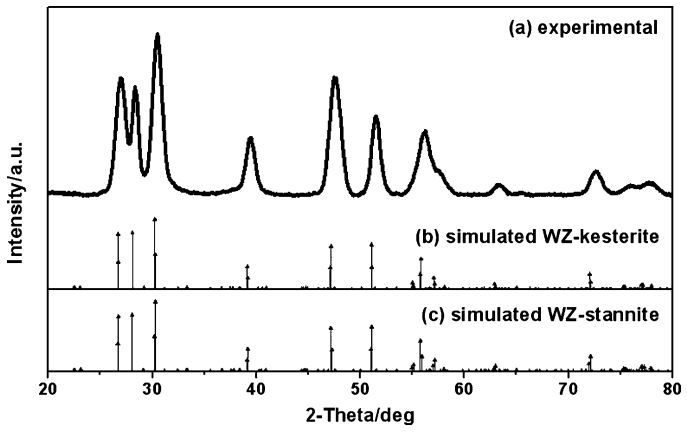


Figure 3. a) XRD pattern of the as-obtained CZTS nanocrystals. b) and c) are simulated XRD patterns of CZTS having the WZ-kesterite and the WZ-stannite structures, respectively.

  

fraction patterns for their CZTS nanocrystals and proposed a structure in which the metal cations ($Cu^+$, $Zn^{2+}$ and $Sn^{4+}$) are in complete disorder.[5] Although our experimental pattern agrees well with the simulated diffraction pattern of their proposed structure, the possibility that the WZ-type CZTS structure has an ordered arrangement of cations (i.e., WZ-kesterite and WZ-stannite) cannot be completely ruled out. Note that the known ZB-related tetragonal structures of CZTS (i.e., kesterite and stannite) are cation-ordered structures. Theoretical studies show that although the exchange of $Cu^+$ and $Zn^{2+}$ occupation is energetically inexpensive, the randomization of $Cu^+$ and $Sn^{4+}$ and of $Zn^{2+}$ and $Sn^{4+}$ are energetically costly due to the chemical and size mismatch between these ions.[2a,8] Thus, a cation-disordered CZTS structure in which there is total random occupation of $Cu^+$, $Zn^{2+}$ and $Sn^{4+}$ is thermodynamically less favorable.

As mentioned earlier, the WZ-kesterite and WZ-stannite CZTS structures have been previously predicted on the basis of theoretical calculations.[2f] These cation-ordered WZ-derived structures can be described as a $2\times2\times1$ superstructure of the WZ unit cell. The hexagonal symmetry of the basic WZ cell is reduced to monoclinic (*Pc*, WZ-kesterite) or orthorhombic ($Pmn2_1$, WZ-stannite) depending on the ordering of $Cu^+$ and $Zn^{2+}$ cations (crystal structures are depicted in Figure S3 in the Supporting Information). We have simulated the powder XRD patterns of CZTS exhibiting the WZ-kesterite and the WZ-stannite structures using the theoretical lattice parameters calculated by Chen et al. (see the Supporting Information for details). As one can see in Figure 3, the experimental pattern matches well with the simulated diffraction patterns of both WZ-kesterite and WZ-stannite phases. However, due to the very similar diffraction patterns of the two WZ-derived structures (Figure S4 in the Supporting Information) and the broadening of diffraction peaks due to the small crystallite size, it would be difficult to distinguish between the two phases based on powder XRD data. The same problem has been reported for the ZB-derived kesterite and stannite phases, which also have indiscernible diffraction patterns.[4a,9] Similar to the relation between the two ZB-derived structures, the two WZ derivatives differ only in the distribution of cations, particularly $Cu^+$ and $Zn^{2+}$. Since $Cu^+$ and $Zn^{2+}$ are isoelectronic (i.e., they have the same number of electrons), it is not possible to distinguish between them by X-ray analysis, because they have equal atomic scattering factors. Neutron diffraction has proven to be an effective tool in the structural determination of the ZB-derived CZTS phases, because of the different neutron scattering lengths of $Cu^+$ and $Zn^{2+}$.[10] The application of this technique in the structural investigation of WZ-type CZTS is recommended for future work.

As revealed by first-principles calculations, the thermodynamic stability of the four CZTS structures is in the order: kesterite > stannite > WZ-kesterite > WZ-stannite.[2f] Because the ZB derivatives are thermodynamically more stable than their WZ analogues, it is not surprising that earlier works on the synthesis of CZTS have produced the lower-energy ZB-related structures. In colloidal nanocrystal synthesis, the presence of organic surfactants or capping ligands is known to strongly influence the crystallographic phase, morphology, and growth of the nanocrystals.[11] Thus, the formation of metastable phases can be induced with proper selection of surfactants. The use of different organic surfactants in the synthesis of CZTS nanocrystals was investigated and the results of our experiments are summarized in Table S1 (in the Supporting Information). Our study shows that the presence of long-chain alkanethiols such as hexadecanethiol (HDT) and dodecanethiol (DDT) is pivotal in producing WZ-type CZTS nanocrystals (Figure 3a and Figure S5a-b in the Supporting Information). By contrast, oleylamine (OM) is found to be effective in promoting the formation of the ZB-derived CZTS structure (Figure S5c-d in the Supporting Information). While trioctylamine (TOA) does not influence the crystallographic phase, its use in combination with alkanethiols results in nanocrystals that are well-separated and highly monodisperse.

In order to gain insights into the formation mechanism of our WZ-type CZTS nanocrystals, the growth process in the presence of HDT was monitored as a function of reaction time at 250 °C. The TEM images (Figure 4) and XRD patterns (Figure S6 in the Supporting Information) reveal that at a shorter reaction time ($t=1$ min), two-component nanostructures consisting of $Cu_{1.94}S$ (ca. 10 nm) and WZ-type CZTS (ca. 5 nm) are formed. At a reaction time of 30 min, only WZ-type CZTS nanocrystals that are elongated in shape ($15\times8$ nm) are observed indicating that the $Cu_{1.94}S$ portion has been converted to WZ-type CZTS. Prolonging the reaction time from 30 to 120 min increases the nanocrystal size ($20\times9$ nm). It is worth noting that when $[Cu(dedtc)_2]$ is solely decomposed in the presence of HDT, $Cu_{1.94}S$ is obtained exclusively as the thermolysis product (Figure S7a in the Supporting Information). The above-mentioned observations indicate that the growth process begins with nucleation

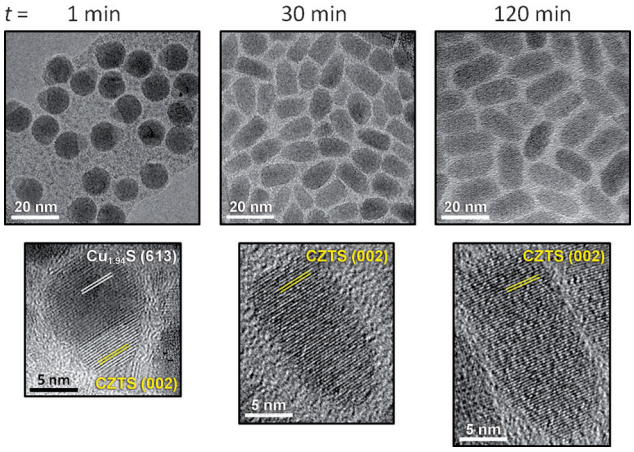


Figure 4. TEM (top) and HRTEM (bottom) images of the nanocrystals obtained at 250 °C in the presence of HDT at varying reaction times: $t=$ 1, 30 and 120 min.

  

of $Cu_{1.94}S$ nanocrystals. This is immediately followed by nucleation and anisotropic growth of WZ-type CZTS onto one side of the $Cu_{1.94}S$ nanocrystals, resulting in $Cu_{1.94}S$–CZTS heterostructured nanocrystals. As the reaction progresses, interdiffusion of the cations between the two components occurs, which eventually leads to purely WZ-type CZTS nanocrystals. This is similar to the previously reported transformation of $Cu_2S$–$CuInS_2$ hybrid nanocrystals to purely WZ-type $CuInS_2$ nanorods.[12]

As the binary copper sulfide that initially forms serves as the starting point for the nucleation and growth of CZTS, the crystal structure of the generated CZTS is dictated by the structure of the copper sulfide seed. Binary copper sulfides ($Cu_xS$, $x=1$–2) exist in a variety of phases, which can be influenced by the organic surfactant used in the synthesis.[13] In our synthesis using HDT, the $Cu_xS$ that forms is monoclinic $Cu_{1.94}S$ (djurleite), the anion sublattice of which can be described as a hexagonal close packing (hcp) array of sulfur ions. As a result, the CZTS that nucleates and grows onto the initial $Cu_{1.94}S$ exhibits the WZ-related crystal structure, in which the sulfur anions are also in a hexagonal close-packed arrangement. With the similar anionic framework of $Cu_{1.94}S$ and WZ-type CZTS, the interdiffusion of cations between the two materials becomes possible as there is little lattice distortion, resulting in the eventual conversion of the $Cu_{1.94}S$ segment to WZ-type CZTS. The cationic vacancies and the high mobility of Cu ions in nonstoichiometric $Cu_{1.94}S$ are also believed to facilitate the conversion.

When HDT is replaced with OM, ZB-derived tetragonal CZTS is obtained even at shorter reaction times (Figure S8 in the Supporting Information). Note that primary alkylamines, such as OM, are known to hasten the decomposition of metal dithiocarbamate complexes.[14] The formation of ZB-type CZTS instead of the WZ-related polytype tells us that the growth process in the presence of OM does not involve $Cu_{1.94}S$. When $[Cu(dedtc)_2]$ was decomposed solely in the presence of OM, it was found that the binary copper sulfide phase generated is $Cu_{1.8}S$ (digenite), as evidenced by the XRD pattern shown in Figure S7b (in the Supporting Information). Unlike $Cu_{1.94}S$, which has the hcp anionic framework, $Cu_{1.8}S$ has a cubic close packing (ccp) array of sulfur anions.[15] We believe that in the presence of OM, $Cu_{1.8}S$ plays a vital role in inducing the formation of ZB-type CZTS, which has a similar ccp framework of sulfur ions. Interestingly, in the presence of both HDT and OM, thermolysis of $[Cu(dedtc)_2]$ yields a mixture of $Cu_{1.94}S$ and $Cu_{1.8}S$ (Figure S7c in the Supporting Information). Since $Cu_{1.94}S$ and $Cu_{1.8}S$ are both formed, the CZTS produced using this surfactant mixture consists of both WZ- and ZB-derived phases (Figure S9a in the Supporting Information).

We have determined the band gap of our $(15\times8)$ nm-sized WZ-type CZTS nanocrystals from the absorption spectrum shown in Figure S10 (in the Supporting Information). From the plot of the square of $\alpha h\nu$ (in which $\alpha$ = absorption coefficient; $h\nu$ = photon energy) versus the photon energy (inset of Figure S10 in the Supporting Information), $E_g$ is estimated to be 1.55 eV. The observed value is only slightly larger than the band gap reported in the literature for CZTS nanocrystals with the ZB-derived tetragonal structure (i.e., $E_g=1.5$ eV for nanocrystals that are ca. 13 nm in size).[4b] This value falls within the optimum band gap range for solar energy conversion in a single-junction device. The photovoltaic properties of this WZ-related CZTS phase will be the subject of further research.

In summary, nanocrystalline CZTS has been colloidally synthesized through a facile noninjection route, which involves the surfactant-assisted thermolysis of metal dithiocarbamates. The organic surfactant used in the synthesis is found to influence the crystallographic phase of the CZTS nanocrystals. XRD measurements show that the CZTS nanocrystals prepared in the presence of alkanethiols adopt the recently reported WZ-related crystal structure. By contrast, the presence of oleylamine favors the formation of the more widely studied ZB-derived CZTS phase. Our investigation on the formation mechanism of the WZ-type CZTS nanocrystals reveals that the growth process involves the initial formation of $Cu_{1.94}S$ nanocrystals, which serve as the starting point for the nucleation and growth of WZ-type CZTS. From optical absorption data, the band gap of the WZ-type CZTS nanocrystals is estimated to be 1.55 eV, which is optimal for solar cell applications.

## Experimental Section

**Materials**: All starting materials were purchased from commercial sources and used without further purification. Synthesis of copper(II) diethyldithiocarbamate ($[Cu(dedtc)_2]$) and tin(IV) diethyldithiocarbamate ($[Sn(dedtc)_4]$) ($dedtc=(S_2CNEt_2)^-$) was based on previously published procedures.[16] Zinc(II) diethyldithiocarbamate ($[Zn(dedtc)_2]$) was purchased from Aldrich.

**Synthesis of WZ-type CZTS nanocrystals**: In a typical synthesis, $[Cu(dedtc)_2]$ (36.0 mg, 0.1 mmol), $[Zn(dedtc)_2]$ (18.1 mg, 0.05 mmol), $[Sn(dedtc)_4]$ (35.6 mg, 0.05 mmol), hexadecanethiol (5 mL) and trioctylamine (5 mL) were placed in a 50 mL three-neck flask and the reaction mixture was degassed at 100 °C for 20–30 min. The clear yellow solution that formed was then heated under Ar to 250 °C with vigorous stirring. A change in color from yellow to topaz to dark brown was observed at around 220–240 °C. The resulting mixture was kept stirring at 250 °C under Ar for 30 min before placing in a $H_2O$ bath, allowing the mixture to cool to 40 °C. Ethanol was added to precipitate the nanocrystals, and this was followed by centrifugation. The solid obtained was washed thoroughly with hexane and methanol.

**Characterization**: Bright-field transmission electron microscopy (TEM) images were taken using a JEOL 2100 electron microscope operated at an accelerating voltage of 200 kV. The instrument is equipped with an energy-dispersive X-ray (EDX) detector, which was used for elemental analysis. In preparing the specimens, a drop of nanocrystals dispersed in hexane was placed on the surface of a lacey formvar/carbon 300-mesh Cu grid or onto lacey formvar/carbon 200-mesh Ni grid. Energy-filtered TEM (EFTEM) images were obtained using a Gatan Tridiem ER energy filter attached to an FEI Titan TEM with a Schottky electron source, operated at 200 kV. The three-window method was used, where electrons from 30 eV wide energy windows were imaged at the Cu $L_{2,3}$ edge (935–965 eV loss), Sn $M_{4,5}$ edge (485–515 eV) and S $L_{2,3}$ edge (165–195 eV). The Zn $L_{2,3}$ edge (starting at 1020 eV) is only about 90 eV higher in energy than the Cu $L_{2,3}$ edge, so when pre-edge energy windows are selected for the Zn edge, there is a risk of including the first part of the Cu edge that has large intensity variations. To avoid artifacts in the Zn pre-

  

edge determination, narrower energy windows were used (22 eV wide) for Zn mapping, and only the 35 eV before the Zn edge onset was used for determining the background intensity. X-ray photoelectron spectroscopy (XPS) measurements were conducted using a Thermo Fisher Scientific Thetaprobe XPS spectrometer with an $Al_{K\alpha}$ monochromatic X-ray source at 15 kV and 100 W. X-ray diffraction (XRD) patterns were collected on a Bruker GADDS D8 Discover diffractometer using $Cu_{K\alpha}$ radiation (1.5418 Å). Cu/Zn/Sn metal ratio was determined using a Perkin–Elmer Optima 3000 inductively coupled plasma-atomic emission spectrometer (ICP-AES). Room-temperature absorption spectra were recorded using a Shimadzu UV-3150 UV-Vis-NIR spectrophotometer. Samples were dispersed in $CHCl_3$ and loaded into a quartz cuvette.

## Acknowledgements

We thank Dr. R. B. Nellas of ORNL for useful discussions. C.Y. is supported by the NUS NanoCore PhD Scholarship.

**Keywords:** nanostructures · phase control · semiconductors · surfactants · synthesis

[1] a) D. B. Mitzi, O. Gunawan, T. K. Todorov, K. Wang, S. Guha, *Sol. Energy Mater. Sol. Cells* **2011**, *95*, 1421–1436; b) H. Katagiri, K. Jimbo, W. S. Maw, K. Oishi, M. Yamazaki, H. Araki, A. Takeuchi, *Thin Solid Films* **2009**, *517*, 2455–2460; c) K. Tanaka, M. Oonuki, N. Moritake, H. Uchiki, *Sol. Energy Mater. Sol. Cells* **2009**, *93*, 583–587.

[2] a) S. Chen, X. G. Gong, A. Walsh, S. H. Wei, *Appl. Phys. Lett.* **2010**, *96*, 021902; b) S. Chen, X. G. Gong, A. Walsh, S. H. Wei, *Phys. Rev. B* **2009**, *79*, 165211; c) J. Paier, R. Asahi, A. Nagoya, G. Kresse, *Phys. Rev. B* **2009**, *79*, 115126; d) M. Ichimura, Y. Nakashima, *Jpn. J. Appl. Phys.* **2009**, *48*, 090202; e) C. Persson, *J. Appl. Phys.* **2010**, *107*, 053710; f) S. Chen, A. Walsh, Y. Luo, J. H. Yang, X. G. Gong, S. H. Wei, *Phys. Rev. B* **2010**, *82*, 195203.

[3] W. Schäfer, R. Nitsche, *Mater. Res. Bull.* **1974**, *9*, 645–654.

[4] a) Q. Guo, H. W. Hillhouse, R. Agrawal, *J. Am. Chem. Soc.* **2009**, *131*, 11672–11673; b) S. C. Riha, B. A. Parkinson, A. L. Prieto, *J. Am. Chem. Soc.* **2009**, *131*, 12054–12055.

[5] X. Lu, Z. Zhuang, Q. Peng, Y. Li, *Chem. Commun.* **2011**, *47*, 3141–3143.

[6] a) Z. Zhuang, X. Lu, Q. Peng, Y. Li, *Chem. Eur. J.* **2011**, *17*, 10445–10452; b) M. Y. Chiang, S. H. Chang, C. Y. Chen, F. W. Yuan, H. Y. Tuan, *J. Phys. Chem. C* **2011**, *115*, 1592–1599.

[7] a) C. Steinhagen, M. G. Panthani, V. Akhavan, B. Goodfellow, B. Koo, B. A. Korgel, *J. Am. Chem. Soc.* **2009**, *131*, 12554–12555; b) S. R. Hall, J. T. Szymanski, J. M. Stewart, *Can. Mineral.* **1978**, *16*, 131–137.

[8] a) S. Chen, X. G. Gong, A. Walsh, S. H. Wei, *Appl. Phys. Lett.* **2009**, *94*, 041903; b) S. Chen, J. H. Yang, X. G. Gong, A. Walsh, S. H. Wei, *Phys. Rev. B* **2010**, *81*, 245204.

[9] a) Y. Liu, M. Ge, Y. Yue, Y. Sun, Y. Wu, X. Chen, N. Dai, *Phys. Status Solidi RRL* **2011**, *5*, 113–115; b) A. Fischereder, T. Rath, W. Haas, H. Amenitsch, J. Albering, D. Meischler, S. Larissegger, M. Edler, R. Saf, F. Hofer, G. Trimmel, *Chem. Mater.* **2010**, *22*, 3399–3406.

[10] S. Schorr, *Sol. Energy Mater. Sol. Cells* **2011**, *95*, 1482–1488.

[11] a) Y. Li, X. Li, C. Yang, Y. Li, *J. Phys. Chem. B* **2004**, *108*, 16002–16011; b) A. B. Panda, S. Acharya, S. Efrima, Y. Golan, *Langmuir* **2007**, *23*, 765–770; c) J. W. Cho, H. S. Kim, Y. J. Kim, S. Y. Jang, J. Park, J. G. Kim, Y. J. Kim, E. H. Cha, *Chem. Mater.* **2008**, *20*, 5600–5609.

[12] a) S. T. Connor, C. M. Hsu, B. D. Weil, S. Aloni, Y. Cui, *J. Am. Chem. Soc.* **2009**, *131*, 4962–4966; b) M. Kruszynska, H. Borchert, J. Parisi, J. Kolny-Olesiak, *J. Am. Chem. Soc.* **2010**, *132*, 15976–15986.

[13] a) W. P. Lim, C. T. Wong, S. L. Ang, H. Y. Low, W. S. Chin, *Chem. Mater.* **2006**, *18*, 6170–6177; b) M. D. Regulacio, C. Ye, S. H. Lim, M. Bosman, L. Polavarapu, W. L. Koh, J. Zhang, Q. H. Xu, M. Y. Han, *J. Am. Chem. Soc.* **2011**, *133*, 2052–2055.

[14] N. Pradhan, B. Katz, S. Efrima, *J. Phys. Chem. B* **2003**, *107*, 13843–13854.

[15] W. R. Cook, L. Shiozawa, F. Augustine, *J. Appl. Phys.* **1970**, *41*, 3058–3063.

[16] a) C. G. Sceney, J. O. Hill, R. J. Magee, *Thermochim. Acta* **1975**, *11*, 301–306; b) C. S. Harreld, E. O. Schlemper, *Acta Crystallogr. Sect. B* **1971**, *27*, 1964–1969.

Received: November 17, 2011
Published online: February 14, 2012

  

CHEMISTRY
A EUROPEAN JOURNAL

# Supporting Information



## Colloidal Nanocrystals of Wurtzite-Type $Cu_2ZnSnS_4$: Facile Noninjection Synthesis and Formation Mechanism

**Michelle D. Regulacio,[a] Chen Ye,[b] Suo Hon Lim,[a] Michel Bosman,[a] Enyi Ye,[a] Shiyou Chen,[c] Qing-Hua Xu,[b] and Ming-Yong Han*[a, d]**

chem_201103635_sm_miscellaneous_information.pdf

**Table S1.** Resulting phase and morphology of CZTS nanocrystals prepared by thermally decomposing the metal dithiocarbamate precursors in varying organic surfactants.*

| Surfactants† (Total Volume = 10 mL) | CZTS phase (ZB- or WZ-derived) based on XRD pattern⊥ | Morphology⊥ |
|---|---|---|
| **A.** HDT + TOA (5 mL each) | WZ (Figure 3a) | elongated nanocrystals (Figure 1a) |
| **B.** DDT + TOA (5 mL each) | WZ (Figure S5a) | elongated nanocrystals (Figure S5e) |
| **C.** OM + TOA (5 mL each) | ZB (Figure S5c) | agglomerated particles (Figure S5g) |
| **D.** HDT + OA (5 mL each) | WZ (Figure S5b) | spherical + elongated nanocrystals (Figure S5f) |
| **E.** OM + OA (5 mL each) | ZB (Figure S5d) | agglomerated particles (Figure S5h) |
| **F.** HDT + OM (5 mL each) | WZ + ZB (Figure S9) | elongated nanocrystals that are highly polydisperse (Figure S9a, inset) |

*Mixture was degassed at 80–100 °C prior to heating to 250 °C under Ar, and was then kept at 250 °C for 30 min with vigorous stirring before cooling to 40 °C.
†HDT = hexadecanethiol; TOA = trioctylamine; DDT = dodecanethiol; OM = oleylamine; OA = oleic acid.
⊥XRD patterns and TEM images are shown in the Figures specified in the table.

## Supporting Figures

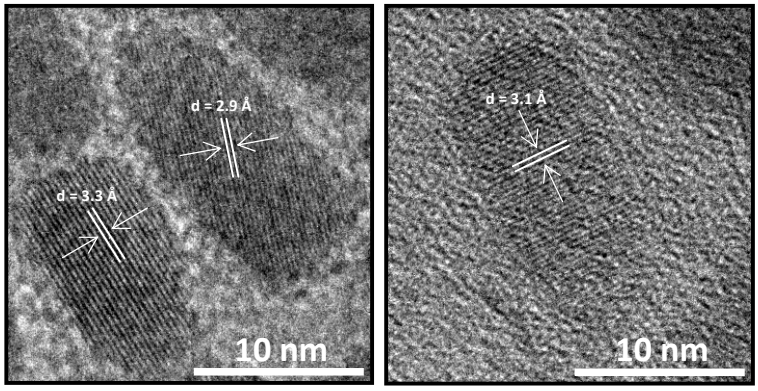


**Figure S1.** High-resolution TEM images of the as-obtained CZTS nanocrystals.

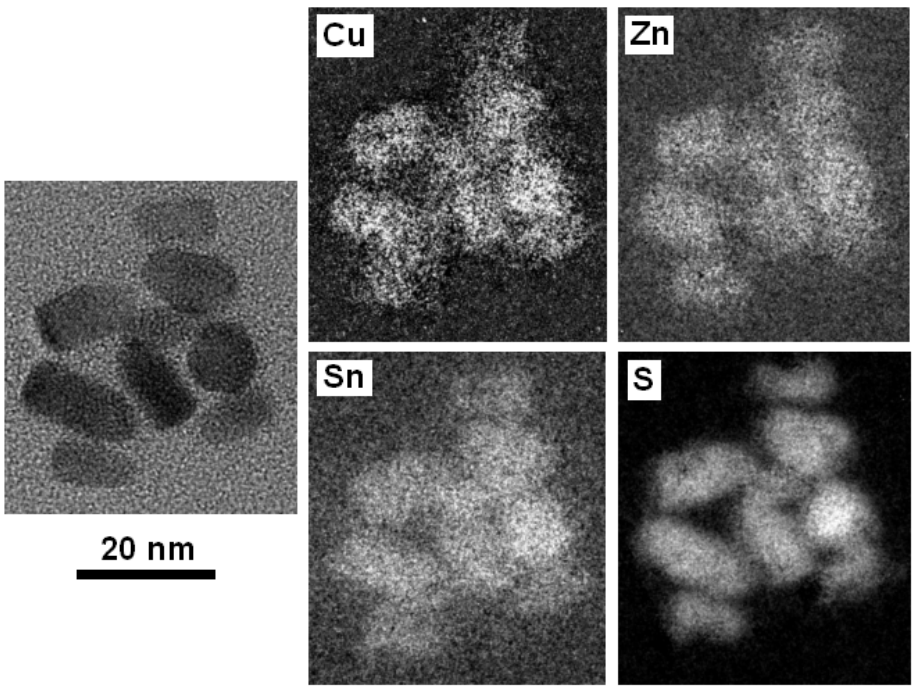


**Figure S2.** Bright-field TEM image (leftmost) and the corresponding energy-filtered TEM images of CZTS nanocrystals showing the Cu, Zn, Sn and S elemental maps.

**Simulated XRD Patterns of the WZ-derived Structures**

The XRD patterns of CZTS exhibiting WZ-kesterite and WZ-stannite structures were simulated using Diamond 3.2 software based on the theoretically determined lattice parameters provided by Chen et al (Reference [2f] in main text). The crystal structures are depicted in Figure S3 whereas the simulated diffraction patterns are shown in Figure S4.

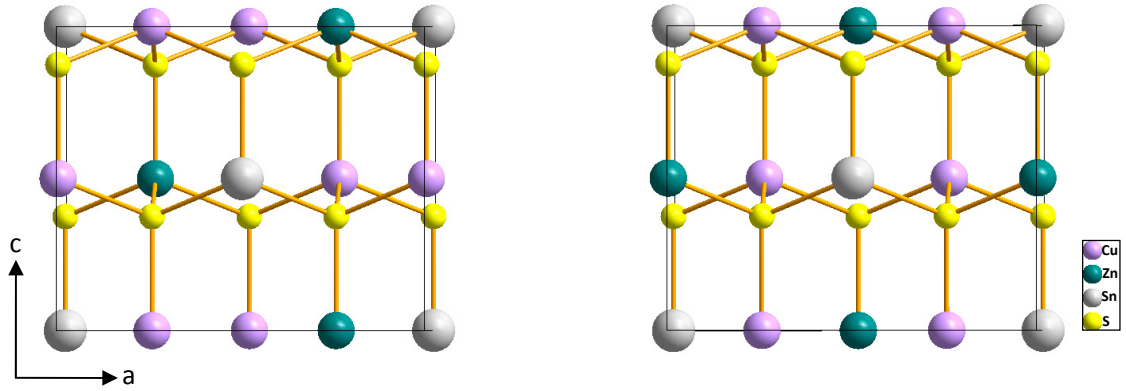


**WZ-kesterite**
monoclinic *Pc* (pseudo-orthorhombic *Pn*)*
*a* = 7.7077 Å; *b* = 6.6630 Å; *c* = 6.3482 Å

**WZ-stannite**
orthorhombic $Pmn2_1$
*a* = 7.6836 Å; *b* = 6.6776 Å; *c* = 6.3519 Å

**Figure S3.** Crystal structures of the WZ-kesterite and WZ-stannite forms of CZTS.

*Note: Since the calculated $\beta$ is nearly 90°, WZ-kesterite is assumed to have a pseudo-orthorhombic unit cell setting described by space group *Pn* (*Acta Cryst*. **1969**, *B25*, 1164–1174).

The experimental lattice parameters, which are calculated based on the (210) and (002) peaks in the powder XRD pattern shown in Figure 3a, are as follows.

*a* = 7.637 Å; *b* = 6.614 Å; *c* = 6.298 Å

The theoretically determined lattice constants are slightly larger than those obtained experimentally. Thus, the peaks in the simulated patterns are slightly shifted to lower 2-theta values relative to the peaks in the experimental pattern. The slight overestimation is common at the GGA-DFT level of theory.

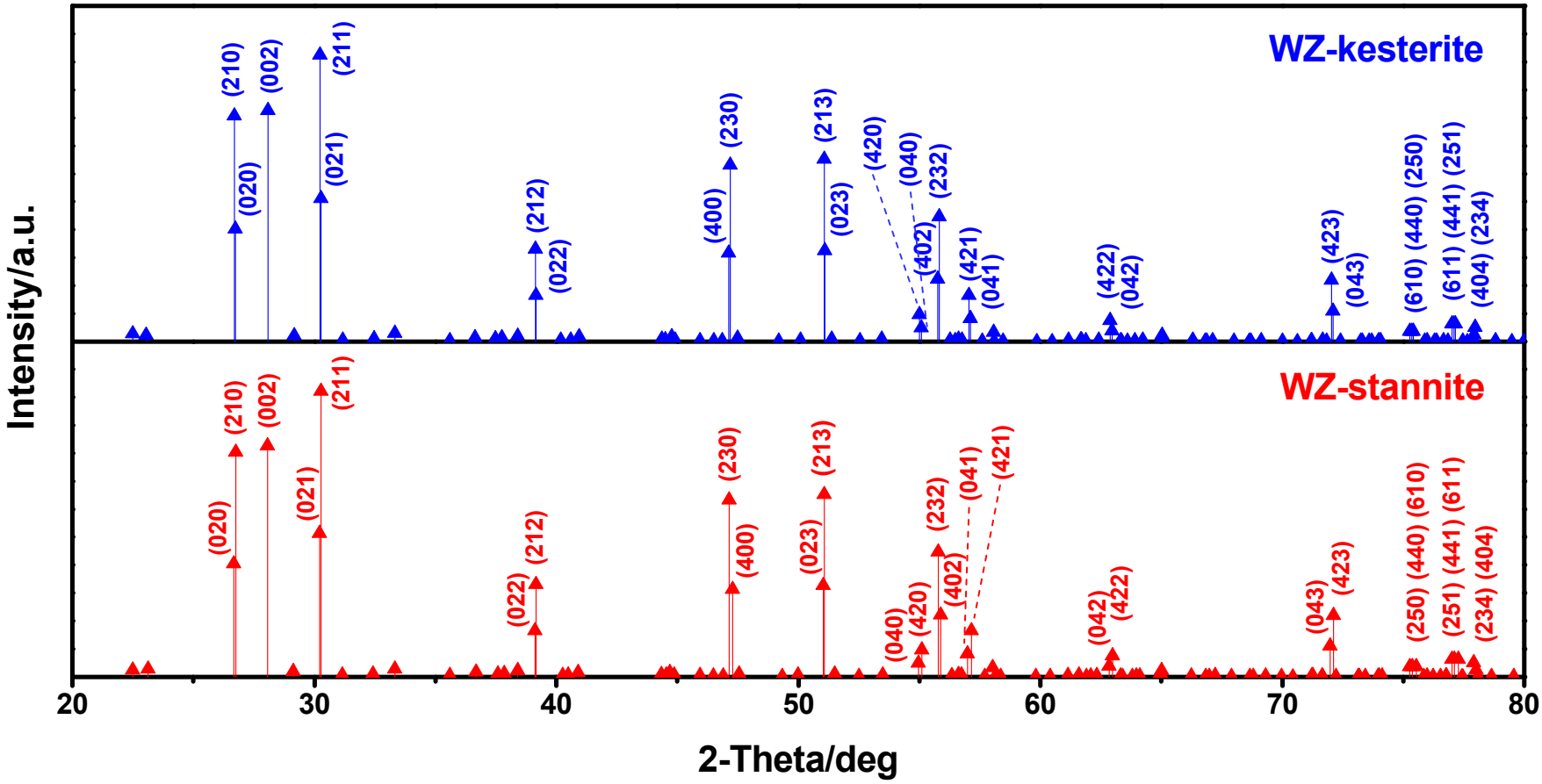


**Figure S4.** Simulated XRD patterns of CZTS exhibiting WZ-kesterite (blue) and WZ-stannite (red) structures. Note that only the (hkl) labels of the most intense peaks are shown.

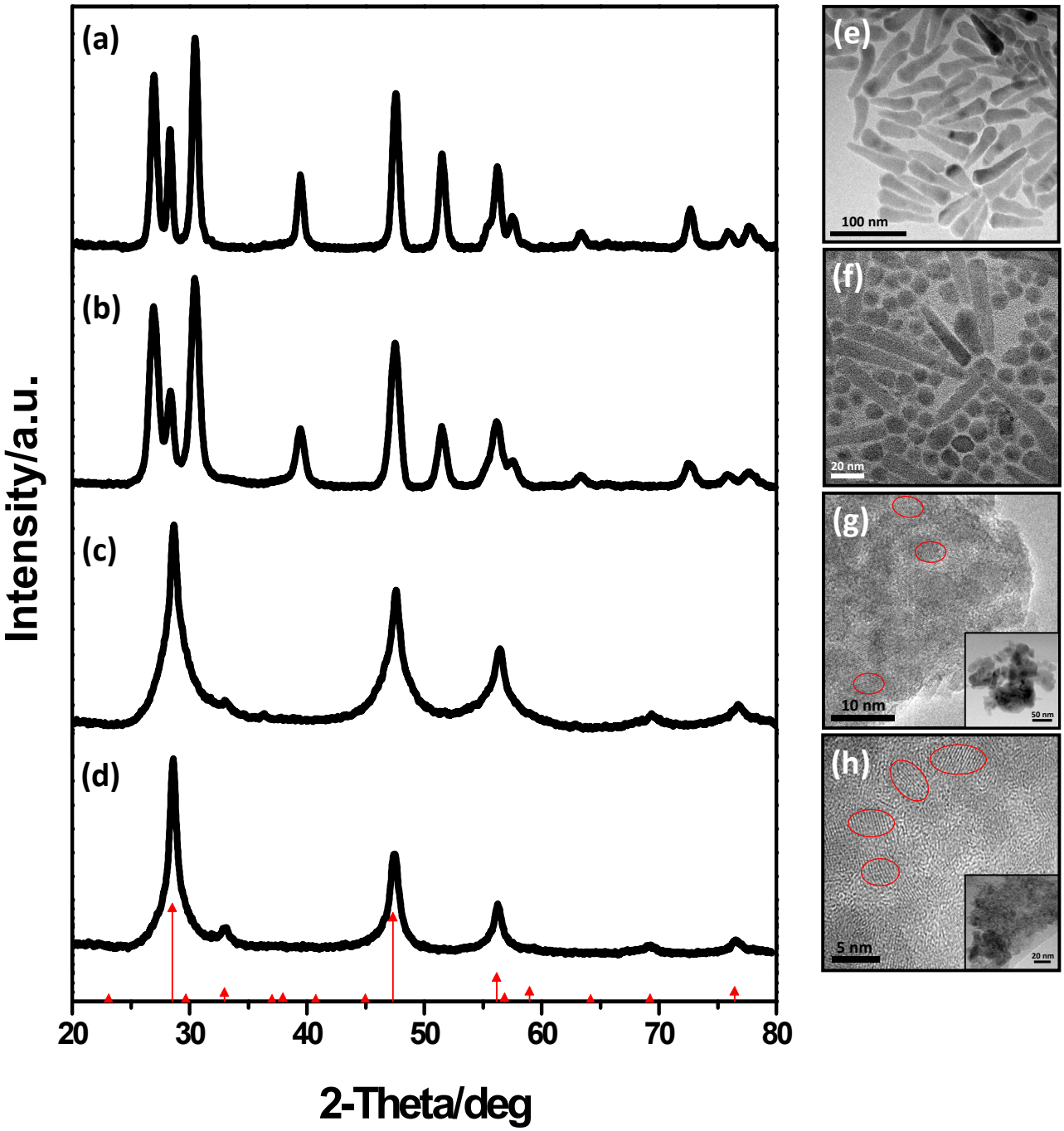


**Figure S5.** XRD patterns (a–d) and TEM images (e–h) of the nanocrystals obtained by thermally decomposing the dithiocarbamate precursors at 250 °C for 30 min in the following surfactant mixtures: DDT + TOA (a, e); HDT + OA (b, f); OM + TOA (c, g) and OM + OA (d, h). Red lines are from standard JCPDS file [26-0575] for $Cu_2ZnSnS_4$ having a ZB-derived tetragonal structure. Red circles on the TEM images are used to highlight the lattice fringes of the agglomerated particles. Lower resolution images are shown in the insets.

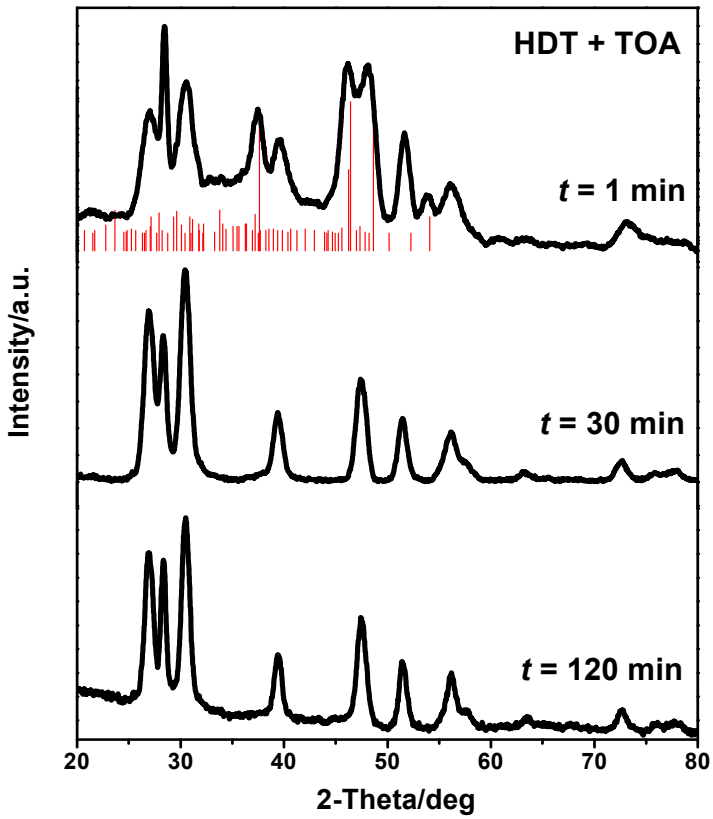


**Figure S6.** XRD patterns of the nanocrystals obtained at 250 °C in the presence of HDT at varying reaction times: $t$ = 1, 30 and 120 min. Red lines are from standard JCPDS file [34-0660] for monoclinic $Cu_{1.94}S$ (djurleite). Note: The formation of the WZ-type CZTS via the initial nucleation of $Cu_{1.94}S$ is attributed to the presence of HDT. We used TOA in combination with HDT to obtain well-separated and highly monodisperse nanocrystals.

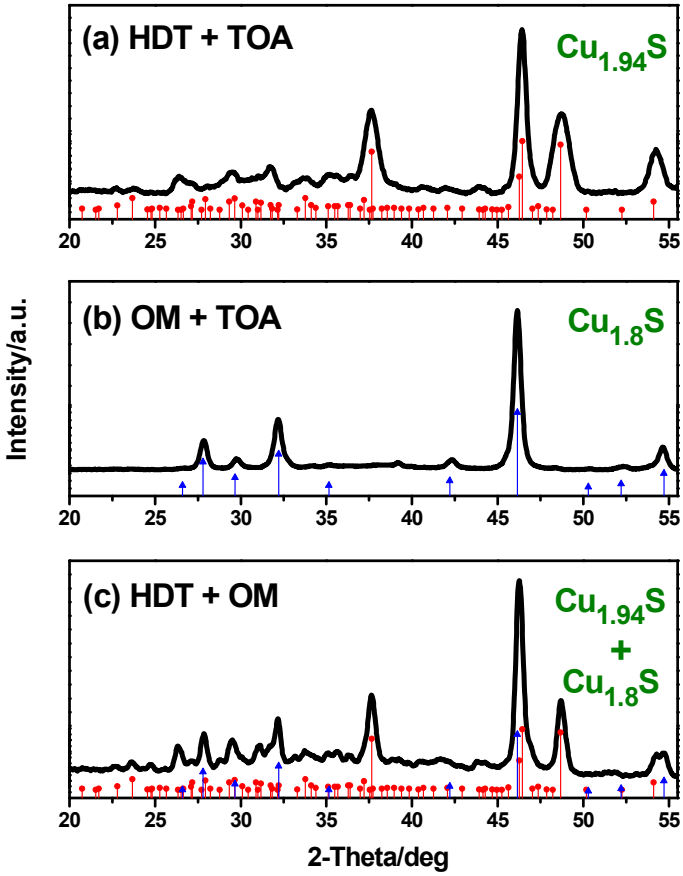


**Figure S7.** XRD patterns of the $Cu_xS$ nanocrystals obtained by thermolysis of $Cu(S_2CNEt_2)_2$ at 250 °C in the following surfactant mixtures: (a) HDT + TOA; (b) OM + TOA; and (c) HDT + OM. Red pattern is from standard JCPDS file for monoclinic $Cu_{1.94}S$ (djurleite) whereas blue pattern is for rhombohedral $Cu_{1.8}S$ (digenite). Note: The formation of $Cu_{1.94}S$ is attributed to the presence of HDT whereas the formation of $Cu_{1.8}S$ is due to the action of OM. $Cu(S_2CNEt_2)_2$ does not readily decompose in pure TOA at 250 °C.

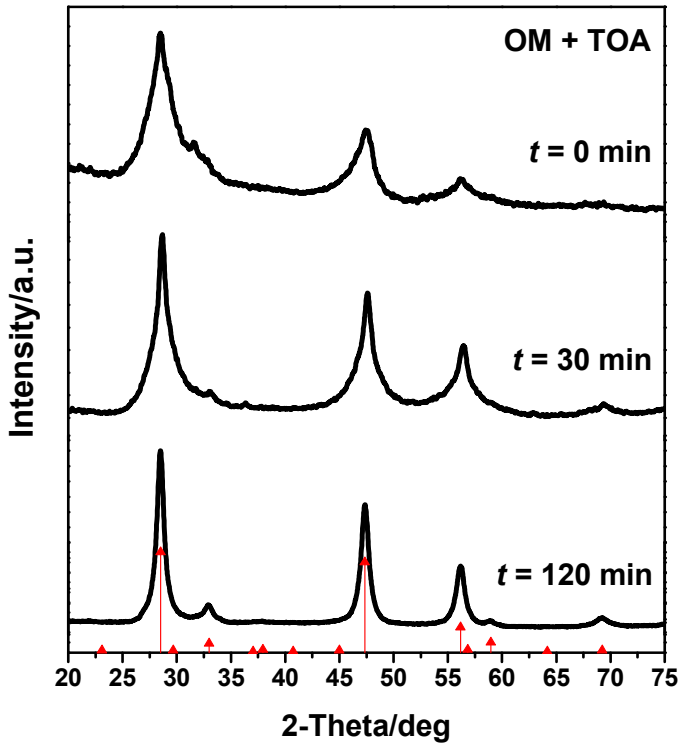


**Figure S8.** XRD patterns of the CZTS nanocrystals obtained at 250 °C in the presence of OM at varying reaction times: $t$ = 0, 30 and 120 min. Red lines are from standard JCPDS file [26-0575] for CZTS having a ZB-derived tetragonal structure.

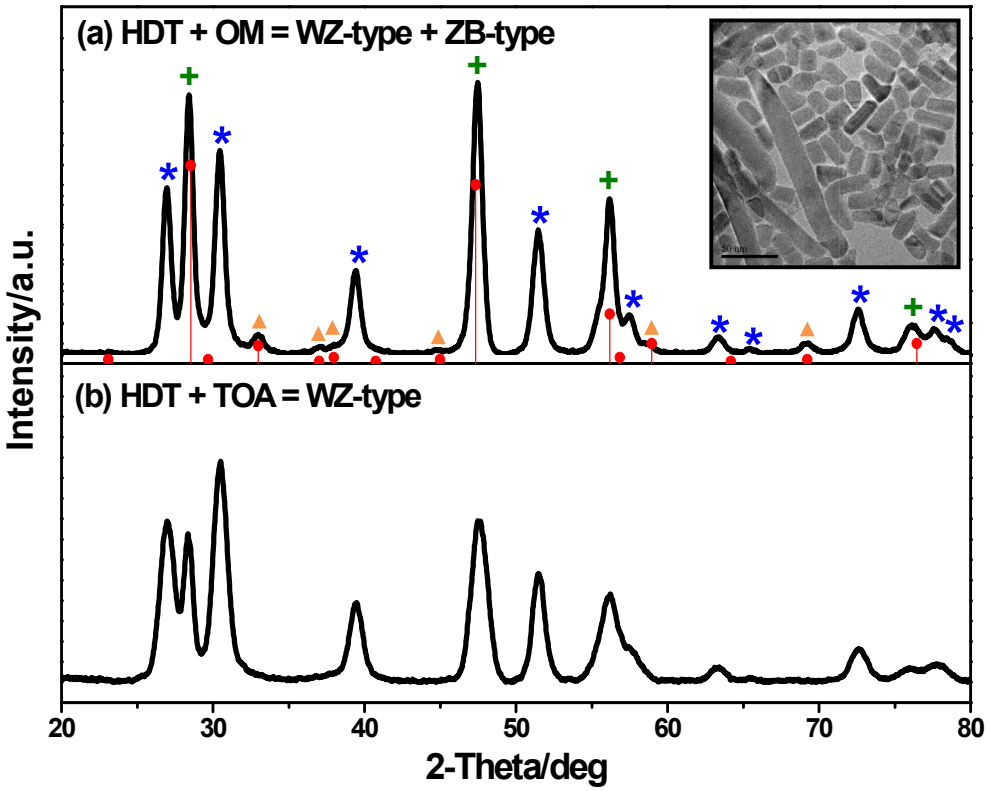


**Figure S9.** (a) XRD pattern of the nanocrystals obtained at 250 °C ($t$ = 30 min) using a surfactant mixture of HDT and OM (TEM image is shown in the inset). (b) XRD pattern of the CZTS nanocrystals prepared using a surfactant mixture of HDT and TOA having a WZ-derived crystal structure (included for comparison). The standard pattern for CZTS having a ZB-derived tetragonal structure is shown in red. The peaks that are solely attributed to the presence of the WZ-derived structure are labeled with blue asterisks whereas those that are mainly attributed to the ZB-derived structure are labeled with orange triangles. A green cross is used to mark the peaks that arise from both the WZ- and ZB-derived structures. Note that these peaks are less intense in (b) where the only phase present is the WZ-type superstructure.

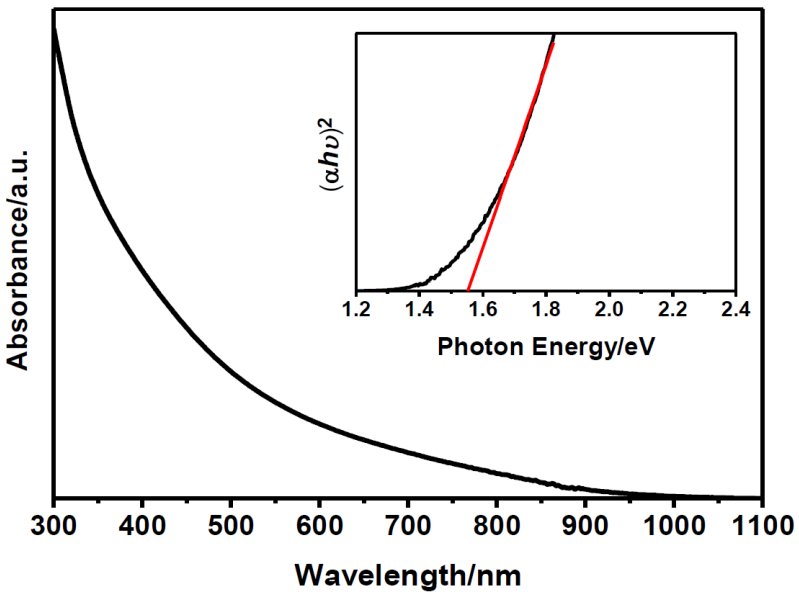


**Figure S10.** Absorption spectrum of WZ-type CZTS nanocrystals. The plot of $(\alpha h\nu)^2$ vs. photon energy (inset) gives a band gap of 1.55 eV.